Langmuir

ARTICLE

pubs.acs.org/Langmuir

Interfacial Immobilization of Monoclonal Antibody and Detection of Human Prostate-Specific Antigen

Xiubo Zhao, Fang Pan, Ben Cowsill, and Jian R. Lu*

Biological Physics Lab, School of Physics and Astronomy, University of Manchester, Schuster Building, Oxford Road, Manchester M13 9PL, United Kingdom

Luis Garcia-Gancedo and Andrew J. Flewitt

Electrical Engineering Division, University of Cambridge, Cambridge CB3 0FA, United Kingdom

Gregory M. Ashley and Jikui Luo

Centre for Materials Research & Innovation, University of Bolton, Deane Road, Bolton BL3 5AB, United Kingdom

ABSTRACT: Antibody orientation and its antigen binding efficiency at interface are of particular interest in many immunoassays and biosensor applications. In this paper, spectroscopic ellipsometry (SE), neutron reflection (NR), and dual polarization interferometry (DPI) have been used to investigate interfacial assembly of the antibody [mouse monoclonal anti-human prostate-specific antigen (anti-hPSA)] at the silicon oxide/water interface and subsequent antigen binding. It was found that the mass density of antibody adsorbed at the interface increased with solution concentration and adsorption time while the antigen binding efficiency showed a steady decline with increasing antibody amount at the interface over the concentration range studied. The amount of antigen bound to the interfacial immobilized antibody reached a maximum when the surface-adsorbed amount of antibody was around 1.5 mg/m^2. This phenomenon is well interpreted by the interfacial structural packing or crowding. NR revealed that the Y-shaped antibody laid flat on the interface at low surface mass density with a thickness around 40 Å, equivalent to the short axial length of the antibody molecule. The loose packing of the antibody within this range resulted in better antigen binding efficiency, while the subsequent increase of surface-adsorbed amount led to the crowding or overlapping of antibody fragments, hence reducing the antigen binding due to the steric hindrance. In situ studies of antigen binding by both NR and DPI demonstrated that the antigen inserted into the antibody layer rather than forming an additional layer on the top. Stability assaying revealed that the antibody immobilized at the silica surface remained stable and active over the monitoring period of 4 months. These results are useful in forming a general understanding of antibody interfacial behavior and particularly relevant to the control of their activity and stability in biosensor development.

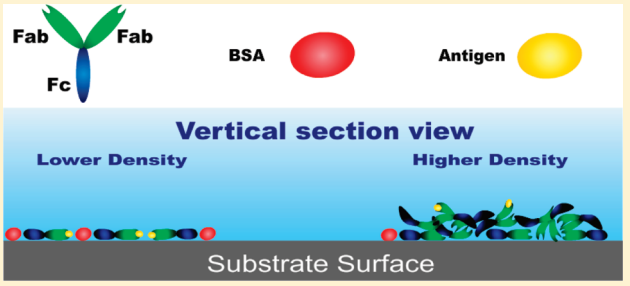

1. INTRODUCTION

Antibodies and antigens have been increasingly used as biomarkers for many biotechnological and biomedical applications such as pregnancy tests and cancer diagnostics. Most of the applications rely on the immobilization of antibodies onto different support interfaces for the purpose of antigen detection. However, in many instances, antigen binding efficiency was dramatically reduced upon interfacial antibody immobilization.[1] Therefore, mechanistic understanding of the interfacial behavior of antibodies and searching of the key factors affecting their antigen binding capacity are very helpful in improving their performance in many technological applications.[2]

The Y-shaped antibody is bivalent. It has two antigen binding fragments (Fab) and one crystallizable fragment (Fc) with its crystalline dimensions approximately 142 × 85 × 38 Å^3.[3] Antigen binding site is often called the variable domain (Fv) as the sequence of Fv varies in different antibodies; it is located at the far end of each Fab fragment. When an antibody is adsorbed or immobilized onto a solid substrate, it can adopt four exemplar molecular orientations: end-on (Fc attached to the support), head-on (Fabs attached to the support), sideways-on (one Fc and one Fab attached to the support), and flat-on (all three fragments attached to the support). In many cases, the actual orientation on a given surface may be a combination of these.[2,4,5] Different molecular interfacial orientations will result in different antigen binding efficiencies or capacities associated with steric hindrances. Better antigen binding capacities can be obtained if

Received: January 17, 2011
Published: May 25, 2011

the Fv area is orientated toward the solution side (end-on), which is clearly the preferred orientation. On the other hand, the efficiency will be reduced if the Fv area is sterically hindered or buried. Optimization of antibody orientation during interfacial immobilization will hugely improve detection sensitivity. Although antibodies can be immobilized through chemical bonding, protein G support, and other more elaborate interfacial molecular engineering,[1,6−9] most practical applications at the industrial scale execute this process by direct spreading or adsorption from solution. It is hence of both foundational and practical significance to establish the relationship between molecular orientations at the interface and antigen binding efficiency for physically adsorbed antibodies.

Prostate cancer is a major cancerous disease in male population and accounts for about 10% of deaths from cancers.[10−12] Its early detection can save millions of lives. Monitoring the prostate-specific antigen (PSA) level in serum is by far the most commonly used approach. PSA is a 34 kDa serine protease synthesized by the prostate gland and has been used as a premier oncological marker due to the lack of real alternative markers of prostate cancer. The total PSA (tPSA) in serum includes both free PSA (fPSA, MW 34 000) and its complexes with various proteinase inhibitors. The complexes with α_1-antichymotrypsin (PSA−ACT, MW 90 000) and α_2-macroglobulin (PSA−AMG) are the two major forms, with the former predominant.[11] Therefore, quantitative detection of fPSA and PSA−ACT can effectively help diagnose prostate cancer. However, the low cutoff limit of the PSA (2.5−4 ng/mL) challenges current detection methods.[12,13] Techniques such as surface plasmon resonance (SPR), quartz crystal microbalance (QCM), electrochemical signal transduction, and microcantilever have all been explored for the detection of PSAs.[12,14] Many approaches including self-assembled monolayers (SAM), biotinylation, fluorescent labeling, protein linkers or ligands, nanoparticle conjugates, and secondary antibodies have been developed to improve detection sensitivity.[10,11,15−22] Among these different approaches, however, label-free detection methods are of interest for future biosensor applications.[23,24] We have recently demonstrated that neutron reflection (NR) is one of the techniques that can effectively determine antibody molecular orientations at the solid/water interfaces.[2,25,26] In this paper, spectroscopic ellipsometry (SE), NR, and dual polarization interferometry (DPI) have been combined to investigate the interfacial assembly of PSA antibody [mouse monoclonal anti-human prostate-specific antigen (anti-hPSA)] at the silicon oxide/water interface and the subsequent in situ antigen binding. The direct determination of in situ interfacial antibody orientation and its relationship to antigen binding is an important step in optimizing biosensor efficiency.

2. EXPERIMENTAL SECTION

2.1. Materials. Silicon ⟨111⟩ wafers were purchased from Compart Technology Ltd. The phosphate buffers were made from Na_2HPO_4 and NaH_2PO_4 (Sigma) with total ionic strength fixed at 20 mM. Decon90 solution was supplied by Decon Laboratories Limited, E. Sussex, U.K. Mouse monoclonal anti-human prostate-specific antigen (anti-hPSA) (catalog no. 7820-0217) and native human prostate-specific antigen (hPSA) (catalog no. 7820-0604) were purchased from AbD Serotec, Oxford, U.K. The concentrations of the antibody and antigen were determined by UV at A_{280} with coefficients of 1.4 for the antibody and 1.84 for the antigen.[27] Bovine serum albumin (BSA) was purchased from Sigma. All samples were used as supplied.

2.2. Spectroscopic Ellipsometry. The principle of ellipsometry has been described in our previous work.[28,29] Silicon wafers were cut into 12×12 mm^2 pieces for use in the ellipsometric cell fitted with a pair of fused quartz windows[30] specially designed for solid/liquid interface measurements. The incoming and exiting beams were at 70° to the surface normal and the windows were aligned to be perpendicular to the two beams. Wafers were cleaned with 5% (v/v) Decon 90, rinsed with plenty of ultra-high-quality water, and dried, giving good hydrophilicity. The thickness of the oxide layer was 12 ± 2 Å as determined by ellipsometry. Interfacial adsorption of the antibody, BSA blocking, and antigen binding were carried out by using Jobin-Yvon UVISEL spectroscopic ellipsometer with a wavelength range between 300 and 600 nm. Data were analyzed by use of software DeltaPsi II developed by Jobin-Yvon Ltd.

2.3. Neutron Reflection. NR measurements were carried out on the SURF reflectometer at ISIS Neutron Facility, Rutherford Appleton Laboratory (RAL), Oxford, U.K., with neutron wavelength ranging from 0.5 to 6.5 Å. A sample solution of about 2 mL was filled into a cell[31,32] made by clamping a transparent Perspex trough against the polished face of a silicon ⟨111⟩ block with surface dimensions of 6×5 cm^2 (the silicon block is 1.2 cm thick). The sample cell was mounted on a goniometer stage linked to a control computer terminal. The neutron beam was defined by two sets of horizontal and vertical slits placed before the sample cell, providing a typical beam illuminating area around 4×3 cm^2 on the center of the polished surface. The neutron beam entering the small face of the silicon block was reflected from the solid/solution interface, exited from the opposite end of the small face, and collected by the detector. Each reflectivity was carried out at three incidence angles of 0.35°, 0.8°, and 1.8° and the resulting reflectivity profiles were combined to cover a wave vector (Q) range between 0.012 and 0.5 Å^{-1}. Reflectivity profiles below the critical angle were theoretically equal to unity, and all the data measured were scaled accordingly. Constant background was subtracted by use of the average reflectivity between 0.3 and 0.5 Å^{-1}. The background was found to be typically around 2×10^{-6} in D_2O. Note that silicon (and silicon wafers for SE) bears a native oxide layer. Its thickness and composition were carefully characterized before any adsorption measurements proceeded.

2.4. Dual Polarization Interferometry. Measurements were performed on the Analight Bio200 dual polarization interferometer (Farfield Sensors Ltd., Manchester, U.K.). The instrument undertook real-time monitoring of time-dependent adsorption onto a bare silicon chip surface doped with nitride. It simultaneously records the thickness, mass, density, and refractive index of the interfacially adsorbed layers. The working principle of DPI and its data analysis have been described in a recent work on lysozyme adsorption.[33] A PHD2000 (Harvard Apparatus) pump was used to provide liquid injection. The DPI was calibrated with 80% ethanol in water and rinsed with phosphate buffer before use. The experiment was started by injection of the antibody solution, followed by incubation, rinsing of phosphate buffer, BSA blocking, buffer rinsing, antigen binding, and buffer rinsing again. Data were then analyzed with Analight Bio Software.

2.5. Stability of Immobilized Antibody. Silicon wafers were cleaned and the thicknesses of the wafers were determined by ellipsometry as described above. Antibody was adsorbed onto the clean silica wafer surface and dried by N_2 after buffer wash. The adsorption was undertaken from 20 mg/L antibody solution for 2 min, resulting in a surface-adsorbed amount of 1.2 ± 0.1 mg/m^2 after buffer wash. Wafers were then stored in clean sealed containers and left at room temperature. BSA blocking and antigen binding experiments were subsequently conducted after different time intervals (every 3−4 weeks) for a period of 4 months.

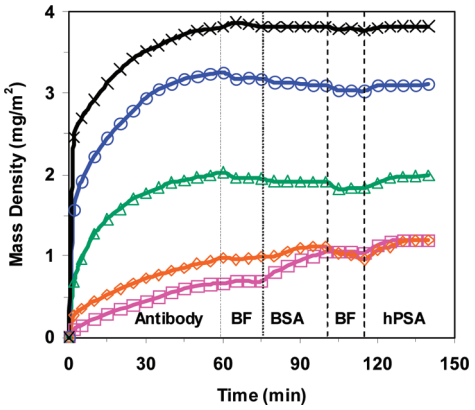

Figure 1. Adsorption of anti-hPSA antibody at 2 (□), 5 (◇), 10 (Δ), 20 (○), and 50 (×) mg/L at the SiO_2/buffer interface followed by buffer wash (BF), BSA (50 mg/L) blocking, buffer wash, and hPSA (5 mg/L) antigen binding. Phosphate buffer at I = 20 mM, pH 7, was used throughout the experiments.

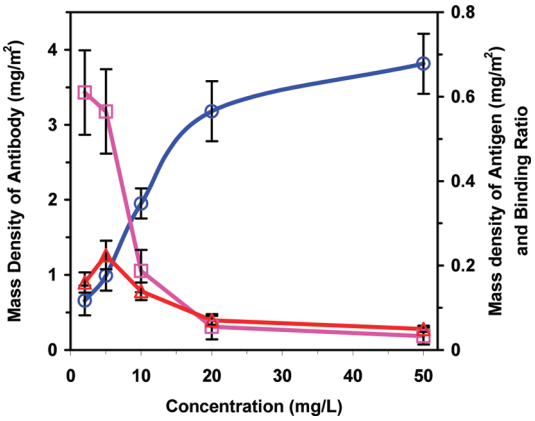

Figure 2. Surface-adsorbed amount of antibody (○, left axis), antigen binding amount (Δ, right axis), and binding ratio (□, right axis) at different antibody concentrations. The surface-adsorbed amounts of antibody were all at 60 min.

3. RESULTS AND DISCUSSION

3.1. Adsorption Dynamics. Spectroscopic ellipsometry (SE) has been widely used as an effective and convenient method for the detection of biomolecules such as proteins, peptides, and DNA at interfaces.[28,29,34−41] Figure 1 shows typical time-dependent adsorption of the antibody at the SiO_2/buffer interface. Both antibody concentration and adsorption time affect the amount of antibody adsorbed at the interface. At all concentrations studied, the surface-adsorbed amount of the antibody steadily increases with time and then tends to plateau. As the antibody concentration increases, the adsorption tends to plateau faster. After the 30 min adsorption, the rate of increase of the adsorbed amount slowed down, but even after being equilibrated for 1 h, the adsorbed amount did not quite reach the equilibrated plateau. The adsorption was then stopped by gentle rinsing with phosphate buffer for 15 min to wash off the free and loosely adsorbed antibody molecules. As evident from Figure 1, desorption was negligible, indicating the strong interaction between silicon oxide surface and antibody molecules driven by electrostatic interaction. BSA has been widely used as a blocking agent in many immunoassays,[2,20,26] to block any nonspecific adsorption (any adsorption that is not through the specific epitope binding), for example, hydrophobic interaction. At antibody concentrations below 10 mg/L, coadsorption of BSA led to an increase of the surface mass density and the total surface-adsorbed amount. However, as the antibody concentrations were above 10 mg/L or the surface antibody amount was above 2 mg/m^2, little BSA coadsorption occurred. This observation indicated that the surface was not fully covered by the antibody molecules when low antibody concentrations were used. Coadsorption of BSA occupied some of the empty spaces on the surface. At high surface coverage of antibody, for example, above 2 mg/m^2, there were few sites for inducing BSA coadsorption. This finding is consistent with the results obtained from glass beads and silica microparticles by Hoehne et al.,[42] who found that the adsorption monolayer footprints of the three antibodies on these particle surfaces were around 2−3 mg/m^2. As already indicated, the antibody has approximate dimensions of 142 × 85 × 38 Å^3. Each molecule occupies an area around 12 100 Å^2 in a flat-on orientation. An adsorbed mass of 2 mg/m^2 almost fully covers the surface (97%). This interfacial structural feature is well supported by the NR data, as will be shown later.

Figure 2 displays the changes of surface-adsorbed antibody against its bulk concentration. The amount of adsorbed antibody shown here represents the values measured after 60 min adsorption. A dramatic elevation of the antibody surface adsorption was observed when its concentration was below 20 mg/L, above which the extent of increase of the adsorbed amount slowed down and tended to an adsorption plateau, an observation consistent with the recent work of Chen et al.,[20] who studied anti-hCG adsorption against concentrations up to 100 mg/L using SPR. These authors found that the SPR angle increased dramatically from 2 to 20 mg/L. Above this concentration the rate of the SPR angle rise was much slower, indicating the attainment of antibody adsorption plateau.

Also displayed in Figure 2 are the changes of antigen binding at the interface and their binding ratio. The ratio of antigen binding is a measure of binding efficiency, which clearly shows a steady decline with increasing antibody adsorption; the rate of decline matches that of antibody adsorption, consistent with the proposed effect of interfacial packing density. A striking observation is the occurrence of the maximum from the amount of antigen binding. Over low concentrations below 5 mg/L, the surface antibody coverage is low. There is a clear trend of rising antigen binding with increasing antibody adsorption, signifying that there was little adverse effect underlying the access of antigen to surface-immobilized antibody. Increase in the amount of antibody at the interface resulted in a greater amount of antigen bound. Meanwhile, the steric hindrance also increased with increasing amounts of antibody. This process explained the subsequent drop of the binding amount, consistent with the continuous decline of the binding ratio. Thus steric hindrance is clearly very significant in interfacial antibody−antigen recognition. The main features of the findings here are consistent with our previous studies of human chorionic gonadotropin (hCG) antibody systems,[2] in which antibody (anti-β-hCG) adsorption, hCG binding, and the binding ratio showed similar trends.[43]

Note that the rising binding amount reported here occurred when antibody concentrations were very low and this effect tends to be overlooked. In general, the amount of antibody adsorbed increases with adsorption time and solution concentration over the time and concentration ranges discussed above. This

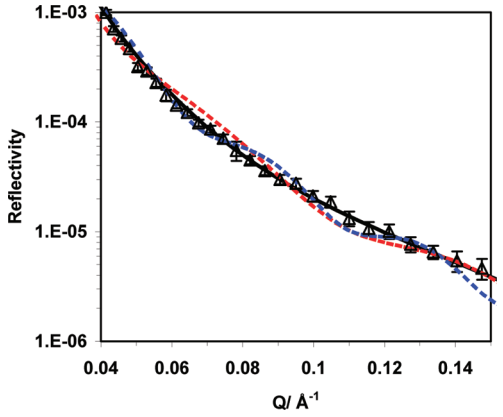

Figure 3. NR profiles at the silicon/D_2O buffer interface at an antibody concentration of 5 mg/L (Δ) in phosphate buffer (I = 20 mM, pH 7 in D_2O). The solid line is the best fit if it is assumed that the antibodies adopted "flat-on" orientations at the interface (τ = 42 Å), while the red and blue dotted lines denote the best fits if it is assumed that the antibodies adopted "side-on" (τ = 85 Å) and "head-on" or "end-on" (τ = 142 Å) orientations at the interface. Prior to the adsorption, the native SiO_2 layer was found to be 12 Å thick with no defects or voids through NR reflection at the silicon/D_2O interface.

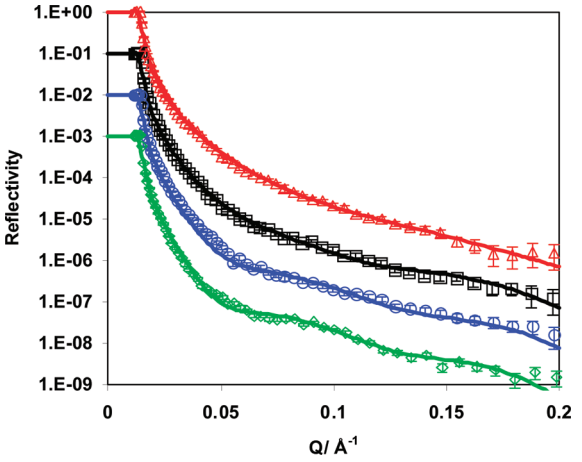

Figure 4. NR profiles at the silicon/D_2O buffer interface with antibody concentrations at 5 (Δ), 10 (□), 20 (○), and 50 mg/L (◇). Phosphate buffer in D_2O at I = 20 mM, pH 7, was used throughout the experiments. Solid lines are the best fits, while symbols denote the measured data. For clarity, the data profiles of 10, 20, and 50 mg/L have been shifted down 1−3 magnitudes along the vertical axis. Parameters obtained by data fitting are shown in Table 1.

phenomenon has also been observed on other surfaces and other antibody−antigen systems.[42−45] As surface packing density of antibody increases, antigen binding tends to drop drastically, a trend consistent with our hPSA observation. Yuan et al.[44] have tried to improve the immobilization capacity of anti-rabbit IgG and antigen binding using chitosan/alginate layer-by-layer self-assembled multilayer films. Their SPR results demonstrated that antigen/antibody binding (and the ratio) decreased with increasing antibody concentration. Le et al.[45] have attached anti-α-hCG to surface substrate through *N*-hydroxysuccinimide. They also found that an increase in surface-adsorbed anti-α-hCG resulted in the reduction of hCG binding efficiency.

3.2. Interfacial Structures. Neutron reflection (NR) is powerful at detecting the thickness and composition of molecular layers or nanofilms with sensitivity down to 2−3 Å.[5,46,47] It has been widely used for studying biological molecules such as DNA,[28,48] proteins,[4,5,49−52] peptides,[36,53,54] and lipids.[32,55,56] Information about the conformational orientations of these biomolecules can be derived from comparing the interfacial structures of the layers with molecular dimensions.

In this work, neutron reflection was carried out with well-polished silicon as substrate. The thickness of the native oxide layer on silicon surface was found to be 12 ± 2 Å from neutron reflectivity measured at the silicon/D_2O interface. No roughness was required to fit the layer, indicating a high degree of surface smoothness. Figure 3 shows the NR profile (Δ) of antibody adsorption at 5 mg/L in 20 mM phosphate buffer in D_2O, pH 7. As the molecules might adopt different orientations at the interface, data were fitted by use of a monolayer model but it was assumed that the molecules adopted "flat-on" (black solid line), "side-on" (red dotted line), and "head-on" or "end-on" (blue dotted line) orientations. Only the monolayer with a thickness of 42 ± 2 Å could fit the measured profile. This thickness corresponds to the short axial length of the antibody molecule, showing that the molecules adopted the "flat-on" orientation at low concentrations. Other models using thicknesses of 85 or 142 Å, corresponding to the other two axial lengths, with varying volume fractions (matching different scattering length densities) failed to fit the measured data. This observation is highly consistent with the published results from other antibodies.[2,5,25,43] NR has previously been used to determine the surface orientation of anti-β-hCG antibody at the SiO_2/water interface.[2,25,26] It was found that anti-β-hCG antibody (at both 2 and 10 mg/L) formed a monolayer with a thickness of 40 ± 3 Å.[2,25] AFM measurements under liquid conditions also revealed a height profile of about 30 Å, slightly less than the short axial length of the antibody, probably due to the compression of the AFM tip causing structural deformation of the adsorbed protein.[25,43] Hoehne et al.[42] also revealed that their two antibodies adsorbed onto the glass surface both had layer thicknesses of ∼4 nm.

The molecular volume fraction (φ) in the layer can be obtained through

$$\varphi_p = \frac{\rho - \rho_w}{\rho_p - \rho_w} \quad (1)$$

where ρ, ρ_p, and ρ_w are the scattering length densities (SLDs) for the layer, the proteins (3.4×10^{-6} Å^{-2} for antibody, 3.3×10^{-6} Å^{-2} for BSA, and 3.1×10^{-6} Å^{-2} for hPSA, all in D_2O), and the water (6.35×10^{-6} Å^{-2} for D_2O), respectively. The labile hydrogens in these proteins were assumed to be fully exchangeable with the solvent. Area per molecule (A) can be expressed as

$$A = \frac{V_p}{\tau \varphi_p} \quad (2)$$

where V_p is the volume of the protein. Surface mass density or adsorbed amount Γ (in milligrams per square meter) can be obtained from

$$\Gamma = \frac{MW}{6.02A} \quad (3)$$

where MW is the molecular mass of the protein in grams per mole and A is in square angstroms.

dx.doi.org/10.1021/la201245q |*Langmuir* 2011, 27, 7654–7662

Table 1. Structural Parameters of Antibody Layers Adsorbed at the Silicon/Buffer Interface[a]

concn (mg·L^{-1})	τ (Å)	($\rho \pm 0.05$) × 10^{-6} (Å^{-2})	$\varphi \pm 0.02$	A (Å^2)	$\Gamma \pm 0.2$ (mg·m^{-2})
5	42 ± 2	5.95	0.14	30 900	0.81
10	12 ± 2	5.7	0.22	13 736	1.8
	25 ± 2	5.5	0.288		
	35 ± 3	6.1	0.085		
20	12 ± 2	5.7	0.22	9263	2.8
	30 ± 2	5.2	0.39		
	28 ± 3	5.8	0.186		
50	12 ± 2	5.5	0.288	7117	3.5
	33 ± 2	5	0.458		
	25 ± 3	5.7	0.22		

[a] Ionic strength = 20 mM, pH 7, in D_2O.

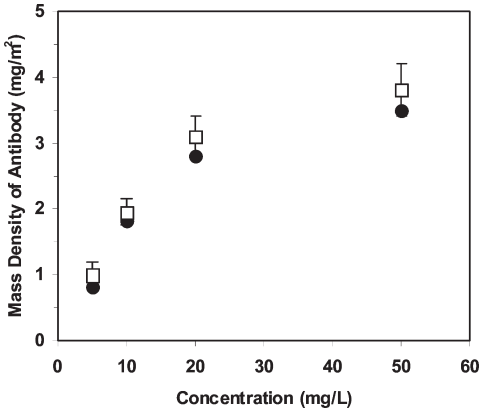

Figure 5. Comparison of surface-adsorbed amounts obtained from ellipsometry (□) and neutron reflection (●) plotted against solution concentration, with all data being measured after 60 min adsorption.

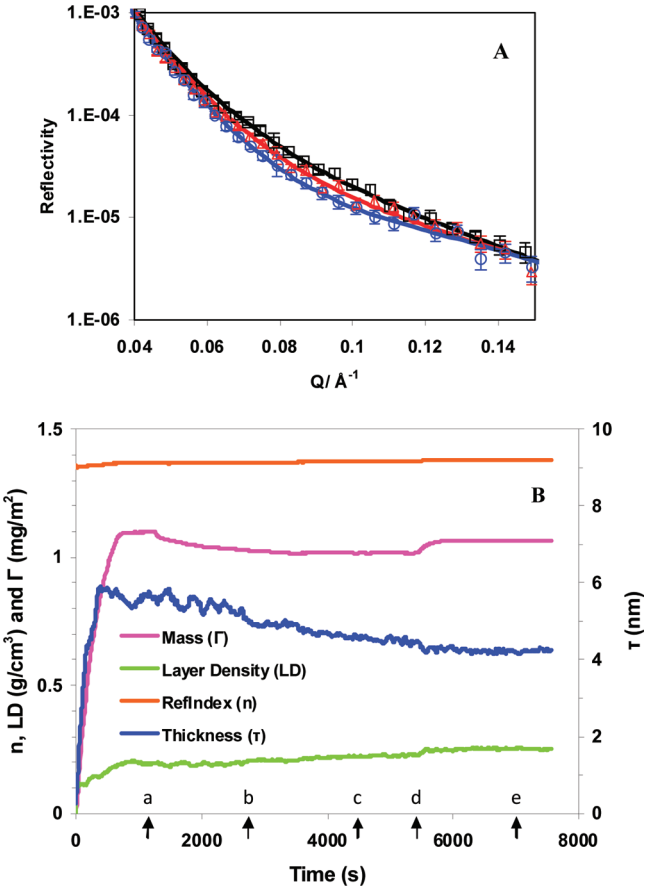

Figure 6. (A) NR profiles measured at the silicon/D_2O buffer interface with antibody adsorption (□), BSA blocking (Δ), and then antigen binding (○). The concentrations for antibody, BSA, and antigen were 5, 50, and 5 mg/L, respectively. For each step, adsorption was allowed for 1 h followed by buffer wash. Phosphate buffer in D_2O at I = 20 mM, pH 7, was used throughout the experiments. Solid lines are the best fits, while symbols represent the measured data. Parameters obtained by data fitting are shown in Table 2. (B) Antibody adsorption from DPI, BSA blocking, and antigen binding under the same solution conditions as used for SE and NR. Arrow indications: (a) buffer wash after antibody adsorption; (b) BSA blocking; (c) buffer wash; (d) antigen binding; (e), buffer wash thereafter.

As demonstrated above, the monolayer model can fit the NR profile at the low antibody concentration of 5 mg/L to the thickness (τ) of about 42 ± 2 Å and the scattering length density (SLD, ρ) of 5.95 × 10^{-6} Å^{-2}. The volume fraction of the layer was found to be 0.14, with the area per molecule around 30 900 Å^2, much bigger than the area occupied by a single antibody. This observation is consistent with the above findings that the surface was not fully covered by the antibody molecules. The presence of gaps or voids between antibody fragments and BSA molecules made it easier for the antigen molecules to access and bind.

To have a systematic understanding of the antibody molecular orientations at the interface and establish the relationship between antibody adsorbed amount and antigen binding ratio, NR experiments were also conducted at several other antibody concentrations. The data are shown in Figure 4, with parameters obtained from data analysis listed in Table 1. At the concentration of 10 mg/L, a single layer could no longer fit the data. A three-layer model has to be used to obtain a good fit. The interior layer was found to have a thickness of 12 ± 2 Å with a volume fraction of 0.22. The middle layer has a thickness of 25 ± 2 Å and a volume fraction of 0.29. The outer layer is much thicker (35 ± 3 Å) but has very few antibodies (φ = 0.085). The main structural feature from such a three-layer model is the coexistence of the different conformational orientations, in particular, the overlapping of the antibody fragments at the interface. The area per molecule reduced to less than 14 000 Å^2, and its reduction signified interfacial crowding. Further increase in the solution concentration to 20 and 50 mg/L resulted in the elevated surface-adsorbed amount and the volume fraction of each layer, consistent with the drop of the area per molecule. The thickness of the layers also varied as well. Although no change in thickness was observed for the interior layer (12 ± 2 Å) over the concentration range from 10 to 50 mg/L, the middle layer thickness increased from 25 ± 2 Å (at 10 mg/L) to 30 ± 2 Å (at 20 mg/L) to 33 ± 2 Å (at 50 mg/L). The thickness of the outer layer, however, was reduced slightly from 35 ± 3 Å (at 10 mg/L) to 28 ± 3 Å (at 20 mg/L) to 25 ± 3 Å (at 50 mg/L). The main observation from this range of variation is, however, the similarity in structural distribution in spite of local variations

dx.doi.org/10.1021/la201245q |*Langmuir* 2011, 27, 7654–7662

Table 2. Optimal Structural Parameters Obtained from Best Fits to Data Shown in Figure 6A

sample/concn (mg·L^{-1})	τ (Å)	($\rho \pm 0.05$) $\times$ 10^{-6} (Å^{-2})	$\varphi_{antibody}$, φ_{BSA}, $\varphi_{antigen}$	$\Gamma_{antibody}$, Γ_{BSA}, $\Gamma_{antigen}$ (mg·m^{-2})	$\Gamma_{total} \pm 0.2$ (mg m^{-2})
antibody/5	42 ± 2	5.95	0.136, 0, 0	0.81, 0, 0	0.81
antibody/5, BSA/50	42 ± 2	5.85	0.136, 0.033, 0	0.81, 0.19, 0	1
antibody/5, BSA/50, antigen/5	42 ± 2	5.70	0.136, 0.033, 0.046	0.81, 0.19, 0.26	1.26

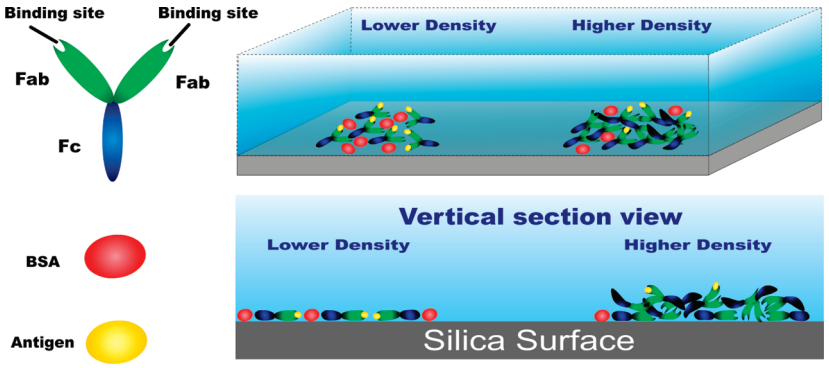

Figure 7. Schematic representation to show adsorbed antibody molecules, BSA blocking, and bound antigen at the silicon/buffer interface bearing a layer of silica or nitrosilica.

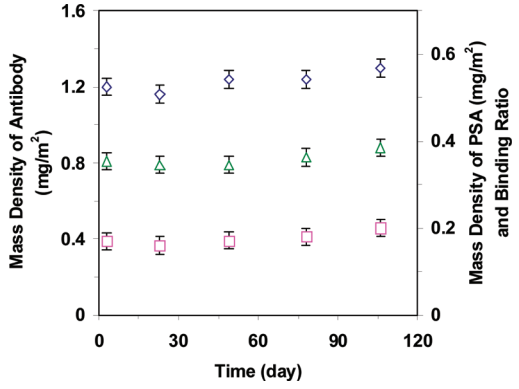

Figure 8. Stability assay of the anti-hPSA antibody immobilized onto the SiO_2 surface. The amounts of antibody (◇, left axis) and antigen (□, right axis) and the binding ratio (Δ, right axis) are displayed against time.

within each layer. The increased volume fraction of each layer and reduced area per molecule show a steady increase of fragment overlapping. The above findings are consistent with the results from DPI studies of anti-CRP (C-reactive protein) antibody by Lin et al.[57] These authors found that the antibody molecules adopt a prone attitude at low concentrations, resulting in a thin layer, while thicker (but probably less dense) layers were observed at higher concentrations. The adsorption from the four concentrations of antibody resulted in surface-absorbed amounts of 0.81, 1.8, 2.8, and 3.5 mg/m^2, respectively, highly consistent with the results obtained from SE measurements (Figure 5). Thus the combined results show that when the concentration is above 10 mg/L or the surface-adsorbed amount is above ~2 mg/m^2, the area per molecule reduced to a value less than the estimated molecular footprint or the limiting cross-sectional area of an antibody molecule, causing a significant decline in the binding efficiency.

3.3. Antigen Binding. Although ellipsometry measurements have shown the adsorbed amount of antibody and the amount of antigen binding, no indication can be gained about the relative location between the antibody and antigen pair. Specifically, it is of interest to find out if the antigens are on top of the antibody layer or inserted into it. NR and DPI experiments have therefore been carried out, with the results shown in Figure 6. In the case of the NR experiment, the antibody was adsorbed at the silicon/D_2O buffer interface (in direct contact with native SiO_2) and left to equilibrate for an hour. NR measurement was carried out after subsequent buffer wash to remove any loosely adsorbed molecules. The data analysis (shown in Table 2) showed the formation of a single layer of antibody at the interface with its thickness, volume fraction, and surface-adsorbed amount at 42 ± 2 Å, 0.136, and 0.81 mg/m^2, respectively. BSA was used as blocking agent, following previous immunoassay studies,[2,25,26,43] to block nonspecific adsorption on the antibody layer. Subsequent NR measurement after buffer wash indicated that BSA blocking did not cause the increased thickness but did have a contribution to the layer SLD, indicating that BSA adsorption occurred via its insertion into the antibody layer. The surface-adsorbed amount and volume fraction of BSA were found to be 0.19 mg/m^2 and 0.033, respectively. Although the values are very low, the detectable amount of BSA adsorption without causing any thickness change indicated that the blocking of nonspecific adsorption sites occurred within the antibody layer. Antigen solution was then applied to the blocked surface. An increase of surface-adsorbed amount (0.26 mg/m^2) was detected with its volume fraction at 0.046 within the layer. Interestingly, the layer thickness was still kept at 42 ± 2 Å, again indicating the insertion of antigen molecules into the layer rather than on top of it.

Similar studies have also been done with DPI because this relatively new analytical technique has already been used for studying interfacial adsorption of a range of biomolecules, including DNA and antibodies.[28,33,57−59] An advantageous feature of DPI is its real-time detection of dynamic adsorption, with simultaneous monitoring of the adsorbed amount, thickness, layer density, and refractive index. The antibody adsorption on

dx.doi.org/10.1021/la201245q |*Langmuir* 2011, 27, 7654–7662

the DPI waveguide (oxynitride surface) resulted in an adsorbed amount of 1.1 mg/m^2, with the thickness around 5−6 nm. The subsequent buffer flow washed off a minor but detectable amount of loosely adsorbed antibody. Fluctuation of the thickness curve and the trend of its steady decline with time indicated molecular reorientation and adjustment at the interface after the fast initial adsorption and the probable compression of solution flow. Over the course of exposure of the antibody layer to different rinsing steps, BSA blocking, and antigen binding, the total layer thickness became eventually constant at ∼4.2 nm, consistent with the finding from the NR experiment. This value is closer to the short axial length of the antibody molecules compared to the value of 2.5 nm from the anti-CRP antibody layer adsorbed at the glutaldehyde-functionalized DPI sensor surface by Lin et al.[57] During this process, the amount of surface-adsorbed antibody varied little before antigen binding, showing that while BSA did not adsorb much, there was little desorption due to buffer rinsing. The lack of BSA adsorption in this case is different from the parallel NR measurement, where a minor but measurable amount of BSA adsorption was detected. The difference could arise from the flow that imposed some shear at the DPI sensor surface. While it is unclear how nitrogen doping could affect surface adsorption characteristics, the initial dynamic adsorption is very different between Figure 1 and Figure 6B, suggesting that flow-associated interfacial shear could speed up interfacial adsorption. However, a jump appeared on the surface-adsorbed mass immediately after the injection of antigen solution into the system and it could not be washed off by the buffer flow, indicating antigen binding onto the antibody. A slight increase of the layer density after antigen injection could also be observed. The increase of layer density without increasing layer thickness also confirmed the insertion of the antigen into the antibody layer. The refractive index, however, did not change much over the whole experimental period, which is reasonable because the three samples were proteins having similar refractive indices.

Based on the above observations, a schematic representation of antibody adsorption, BSA blocking, and antigen binding has been proposed and is shown in Figure 7. At lower surface-adsorbed amounts (e.g., less than 2 mg/m^2), the adsorbed antibody molecules tend to form a flat-on monolayer about 4 nm thick. BSA blocking filled some empty spaces or gaps without affecting layer thickness. The subsequent antigen binding tucked into the ends of Fab fragments, again without increasing layer thickness. At higher surface-adsorbed amounts (e.g., more than 2 mg/m^2), antibodies overlap each other and a lot of binding sites are buried. Only those on the top of the layer are accessible for antigen binding.

3.4. Stability. The stability or bioactivity of the antibody immobilized onto the SiO_2 surface has also been examined and the data are shown in Figure 8. The results clearly demonstrate that the surface-adsorbed antibody molecules still retain bioactivity under dry conditions and ambient temperature over the period (4 months) studied. The net antigen captured by the antibody was 0.18 ± 0.02 mg/m^2 and the binding ratio was 0.36 ± 0.02. This information is particularly useful for future biosensoring applications.

4. CONCLUSIONS

In this study, the interfacial immobilization of a mouse monoclonal antibody (anti-hPSA) and subsequent in situ antigen binding at the silicon/water interface have been investigated. Time-dependent adsorption demonstrated that both antibody concentration and adsorption time affected the surface-adsorbed amount of the anti-hPSA antibody. For the concentrations studied, the adsorption tended to the equilibrated state in about 1 h, with higher concentrations reaching equilibration faster. The surface-adsorbed amount of the antibody on silica surface increased with increasing concentration. In contrast, the antigen binding efficiency as measured by the binding ratio showed an opposite trend, showing the strong effect of surface packing density or steric hindrance, restricting the access of antigens to the binding sites. The amount of antigens grabbed by the antibody molecules at the interface increased to a maximum at a surface-adsorbed amount of antibody around 1.2 mg/m^2 and then showed a steady decline. Over the low surface coverage of antibody, antigen binding did not suffer from any major constraints. Thus, with increasing antibody surface coverage, the amount of antigen bound increased. However, further increase in the surface coverage of antibody resulted in the steric effect. Therefore, the amount of antigen bound started to decrease as a result of steric constraints. Thus, over the high amount of antibody adsorption, only the binding sites on the top layer remained accessible.

NR and DPI results demonstrated that the anti-hPSA antibody adopted a flat-on orientation at the interface over low concentration range, with the antigen molecules inserted into the layer. As solution concentrations became higher, overlapping of the antibody fragments occurred, consistent with the outcome inferred from interfacially adsorbed masses. The surface-immobilized antibodies remained very stable under ambient environment over a period of 4 months studied, making the antibody suitable for future biosensor development.

AUTHOR INFORMATION

Corresponding Author
*Phone 44-161-3063926; e-mail J.Lu@manchester.ac.uk.

ACKNOWLEDGMENT

We thank EPSRC for financial support under Grants EP/F062966/1 and ISIS Neutron Facility at Rutherford Appleton Laboratory for beam time.

REFERENCES

(1) Kausaite-Minkstimiene, A.; Ramanaviciene, A.; Kirlyte, J.; Ramanavicius, A. Comparative study of random and oriented antibody immobilization techniques on the binding capacity of immunosensor. *Anal. Chem.* **2010**, *82*, 6401–6408.

(2) Xu, H.; Lu, J. R.; Williams, D. E. Effect of surface packing density of interfacially adsorbed monoclonal antibody on the binding of hormonal antigen human chorionic gonadotrophin. *J. Phys. Chem. B* **2006**, *110*, 1907–1914.

(3) Silverton, E. W.; Navia, M. A.; Davies, D. R. Three-dimensional structure of an intact human immunoglobulin. *Proc. Natl. Acad. Sci. U.S.A.* **1977**, *74*, 5140–5144.

(4) Lu, J. R.; Zhao, X.; Yaseen, M. Protein adsorption studied by neutron reflection. *Curr. Opin. Colloid Interface Sci.* **2007**, *12*, 9–16.

(5) Zhao, X.; Pan, F.; Lu, J. R. Interfacial assembly of proteins and peptides: recent examples studied by neutron reflection. *J. R. Soc. Interface* **2009**, *6*, S659–S670.

(6) Karyakin, A. A.; Presnova, G. V.; Rubtsova, M. Y.; Egorov, A. M. Oriented immobilization of antibodies onto the gold surfaces via their native thiol groups. *Anal. Chem.* **2000**, *72*, 3805–3811.

(7) Lowe, R. D.; Szili, E. J.; Kirkbride, P.; Thissen, H.; Siuzdak, G.; Voelcker, N. H. Combined immunocapture and laser desorption/ionization mass spectrometry on porous silicon. *Anal. Chem.* **2010**, *82*, 4201–4208.

(8) Ibii, T.; Kaieda, M.; Hatakeyama, S.; Shiotsuka, H.; Watanabe, H.; Umetsu, M.; Kumagai, I.; Imamura, T. Direct immobilization of gold-binding antibody fragments for immunosensor applications. *Anal. Chem.* **2010**, *82*, 4229–4235.

(9) Yakovleva, J.; Davidsson, R.; Lobanova, A.; Bengtsson, M.; Eremin, S.; Laurell, T.; Emnéus, J. Microfluidic enzyme immunoassay using silicon microchip with immobilized antibodies and chemiluminescence detection. *Anal. Chem.* **2002**, *74*, 2994–3004.

(10) Choi, J.-M.; An, J.-Y.; Kim, B.-W. Effect of biolinker on the detection of prostate specific antigen in an interferometry. *Biotechnol. Bioprocess Eng.* **2009**, *14*, 6–12.

(11) Cao, C.; Kim, J. P.; Kim, B. W.; Chae, H.; Yoon, H. C.; Yang, S. S.; Sim, S. J. A strategy for sensitivity and specificity enhancements in prostate specific antigen-alpha1-antichymotrypsin detection based on surface plasmon resonance. *Biosens. Bioelectron.* **2006**, *21*, 2106–2113.

(12) Healy, D. A.; Hayes, C. J.; Leonard, P.; McKenna, L.; O'Kennedy, R. Biosensor developments: application to prostate-specific antigen detection. *Trends Biotechnol.* **2007**, *25*, 125–131.

(13) Schlecht, U.; Gronewold, T. M. A.; Malavé, A.; Tewes, M. Detection of receptor-ligand interactions with an GHz impedance biosensor system. *IEEE Sensors J.* **2007**, *7*, 1680–1684.

(14) Wu, G.; Datar, R. H.; Hansen, K. M.; Thundat, T.; Cote, R. J.; Majumdar, A. Bioassay of prostate-specific antigen (PSA) using microcantilevers. *Nat. Biotechnol.* **2003**, *19*, 856–860.

(15) Liu, F.; Dubey, M.; Takahashi, H.; Castner, D. G.; Grainger, D. W. Immobilized antibody orientation analysis using secondary ion mass spectrometry and fluorescence imaging of affinity-generated patterns. *Anal. Chem.* **2010**, *82*, 2947–2958.

(16) Yuhi, T.; Nagatani, N.; Endo, T.; Kerman, K.; Takata, M.; Konaka, H.; Namiki, M.; Takamura, Y.; Tamiya, E. Gold nanoparticle based immunochromatography using a resin modified micropipette tip for rapid and simple detection of human chorionic gonadotropin hormone and prostate-specific antigen. *Sci. Technol. Adv. Mater.* **2006**, *7*, 276–281.

(17) Kyprianou, D.; Guerreiro, A. R.; Chianella, I.; Piletska, E. V.; Fowler, S. A.; Karim, K.; Whitcombe, M. J.; Turner, A. P. F.; Piletsky, S. A. New reactive polymer for protein immobilisation on sensor surfaces. *Biosens. Bioelectron.* **2009**, *24*, 1365–1371.

(18) Escamilla-Gómeza, V.; Hernández-Santos, D.; González-García, M. B.; Pingarrón-Carrazón, J. M.; Costa-García, A. Simultaneous detection of free and total prostate specific antigen on a screen-printed electrochemical dual sensor. *Biosens. Bioelectron.* **2009**, *24*, 2678–2683.

(19) Liu, X.; Dai, Q.; Austin, L.; Coutts, J.; Knowles, G.; Zou, J.; Chen, H.; Huo, Q. A one-step homogeneous immunoassay for cancer biomarker detection using gold nanoparticle probes coupled with dynamic light scattering. *J. Am. Chem. Soc.* **2008**, *130*, 2780–2782.

(20) Chen, H.; Huang, J.; Lee, J.; Hwang, S.; Koh, K. Surface plasmon resonance spectroscopic characterization of antibody orientation and activity on the calixarene monolayer. *Sens. Actuators, B* **2010**, *147*, 548–533.

(21) Dinh, D. H.; Pascal, É.; Vellutini, L.; Bennetau, B.; Rebière, D.; Dejous, C.; Moynet, D.; Belin, C.; Pillot, J.-P. Novel optimized biofunctional surfaces for Love mode surface acoustic wave based immunosensors. *Sens. Actuators, B* **2010**, *146*, 289–296.

(22) Vareiro, M. M. L. M.; Liu, J.; Knoll, W.; Zak, K.; Williams, D.; Jenkins, A. T. A. Surface plasmon fluorescence measurements of human chorionic gonadotrophin: Role of antibody orientation in obtaining enhanced sensitivity and limit of detection. *Anal. Chem.* **2005**, *77*, 2426–2431.

(23) Wee, K. W.; Kang, G. Y.; Park, J.; Kang, J. Y.; Yoon, D. S.; Park, J. H.; Kim, T. S. Novel electrical detection of label-free disease marker proteins using piezoresistive self-sensing micro-cantilevers. *Biosens. Bioelectron.* **2005**, *20*, 1932–1938.

(24) Kim, A.; Ah, C. S.; Yu, H. Y.; Yang, J.-H.; Baek, I.-B.; Ahn, C.-G.; Park, C. W.; Jun, M. S.; Lee, S. Ultrasensitive, label-free, and real-time immunodetection using silicon field-effect transistors. *Appl. Phys. Lett.* **2007**, *91*, No. 103901.

(25) Xu, H.; Zhao, X.; Grant, C.; Lu, J. R.; Williams, D. E.; Penfold, J. Orientation of a monoclonal antibody adsorbed at the solid/solution interface: A combined study using atomic force microscopy and neutron reflectivity. *Langmuir* **2006**, *22*, 6313–6320.

(26) Xu, H.; Zhao, X.; Lu, J. R.; Williams, D. E. Relationship between the structural conformation of monoclonal antibody layers and antigen binding capacity. *Biomacromolecules* **2007**, *8*, 2422–2428.

(27) Chen, Z.; Prestiglacomo, A.; Stamey, T. A. Purification and characterization of prostate-specific antigen (PSA) complexed to α_1-antichymotrypsin: Potential reference material for international standardization of PSA immunoassays. *Clin. Chem.* **1995**, *41*, 1273–1282.

(28) Zhao, X. B.; Pan, F.; Coffey, P.; Lu, J. R. Cationic copolymer-mediated DNA immobilization: Interfacial structure and composition as determined by ellipsometry, dual polarization interferometry, and neutron reflection. *Langmuir* **2008**, *24* (23), 13556–13564.

(29) Pan, F.; Zhao, X.; Perumal, S.; Waigh, T. A.; Lu, J. R.; Webster, J. R. P. Interfacial dynamic adsorption and structure of molecular layers of peptide surfactants. *Langmuir* **2010**, *26*, 5690–5696.

(30) Tang, Y.; Lu, J. R.; Lewis, A. L.; Vick, T. A.; Stratford, P. W. Swelling of zwitterionic polymer films characterized by spectroscopic ellipsometry. *Macromolecules* **2001**, *34* (25), 8768–8776.

(31) Marsh, R. J.; Jones, R. A. L.; Sferrazza, M.; Penfold, J. Neutron reflectivity study of the adsorption of β-lactoglobulin at a hydrophilic solid/liquid interface. *J. Colloid Interface Sci.* **1999**, *218*, 347–349.

(32) Fragneto-Cusani, G. Neutron reflectivity at the solid/liquid interface: examples of applications in biophysics. *J. Phys.: Condens. Matter* **2001**, *13*, 4973–4989.

(33) Lu, J. R.; Swann, M. J.; Peel, L. L.; Freeman, N. J. Lysozyme adsorption studies at the silica/water interface using dual polarization interferometry. *Langmuir* **2004**, *20*, 1827–1832.

(34) Zhao, X.; Zhang, Z.; Pan, F.; Ma, Y.; Armes, S. P.; Lewis, A. L.; Lu, J. R. DNA immobilization using biocompatible diblock phosphorylcholine copolymers. *Surf. Interface Anal.* **2006**, *38* (4), 548–551.

(35) Zhao, X.; Zhang, Z.; Pan, F.; Ma, Y.; Armes, S. P.; Lewis, A. L.; Lu, J. R. Solution pH regulated interfacial adsorption of diblock phosphorylcholine copolymers. *Langmuir* **2005**, *21*, 9597–9603.

(36) Zhao, X.; Pan, F.; Perumal, S.; Xu, H.; Lu, J. R.; Webster, J. R. P. Interfacial assembly of cationic peptide surfactants. *Soft Matter* **2009**, *5*, 1630–1638.

(37) Zhao, X.; Pan, F.; Lu, J. R. Interfacial immobilization of DNA molecules. *Annu. Rep. Prog. Chem., Sect. C: Phys. Chem.* **2007**, *103*, 261–286.

(38) Zhao, X.; Pan, F.; Lu, J. R. Adsorption of polyethyleneimine characterized by spectroscopic ellipsometry. *Prog. Nat. Sci.* **2005**, *15* (sp), 56–59.

(39) Zhang, Z.; Cao, X.; Zhao, X.; Withers, S. B.; Holt, C. M.; Lewis, A. L.; Lu, J. R. Controlled delivery of antisense oligodeoxynucleotide from cationically modified phosphorylcholine polymer films. *Biomacromolecules* **2006**, *7* (3), 784–791.

(40) Zhang, Z.; Cao, X.; Zhao, X.; Holt, C. M.; Lewis, A. L.; Lu, J. R. Controlled delivery of anti-sense oligodeoxynucleotide from multi-layered biocompatible phosphorylcholine polymer films. *J. Controlled Release* **2008**, *130*, 69–76.

(41) Pan, F.; Zhao, X.; Waigh, T. A.; Lu, J. R.; Miano, F. Interfacial adsorption and denaturization of human milk and recombinant rice lactoferrin. *Biointerphases* **2008**, *3* (2), FB36–FB43.

(42) Hoehne, M.; Samuel, F.; Dong, A.; Wurth, C.; Mahler, H.-C.; Carpenter, J. F.; Randolph, T. W. Adsorption of monoclonal antibodies to glass microparticles. *J. Pharm. Sci.* **2011**, *100*, 123–132.

(43) Wang, X.; Wang, Y.; Xu, H.; Shan, H.; Lu, J. R. Dynamic adsorption of monoclonal antibody layers on hydrophilic silica surface: A combined study by spectroscopic ellipsometry and AFM. *J. Colloid Interface Sci.* **2008**, *323*, 18–25.

(44) Yuan, W.; Dong, H.; Li, C. M.; Cui, X.; Yu, L.; Lu, Z.; Zhou, Q. pH-Controlled construction of chitosan/alginate multilayer film: Characterization and application for antibody immobilization. *Langmuir* **2007**, *23*, 13046–13052.

(45) Le, N. C. H.; Gubala, V.; Gandhiraman, R. P.; Coyle, C.; Daniels, S.; Williams, D. E. Total internal reflection ellipsometry as a label-free assessment method for optimization of the reactive surface of bioassay devices based on a functionalized cycloolefin polymer. *Anal. Bioanal. Chem.* **2010**, *398*, 1927–1936.

(46) Lu, J. R.; Lee, E. M.; Thomas, R. K. The analysis and interpretation of neutron and X-ray specular reflection. *Acta Crystallogr.* **1996**, *A52*, 11–41.

(47) Lu, J. R.; Su, T. J.; Thomas, R. K.; Penfold, J.; Webster, J. Structural conformation of lysozyme layers at the air/water interface studied by neutron reflection. *J. Chem. Soc., Faraday Trans* **1998**, *94*, 3279–3287.

(48) Zhang, J.; Taylor, D. J. F.; Li, P. X.; Thomas, R. K.; Wang, J. B.; Penfold, J. Adsorption of DNA and dodecyl trimethylammonium bromide mixtures at the air/water interface: A neutron reflectometry study. *Langmuir* **2008**, *24* (5), 1863–1872.

(49) Lu, J. R.; Su, T. J.; Georganopoulou, D.; Williams, D. E. Interfacial dissociation and unfolding of glucose oxidase. *J. Phys. Chem. B* **2003**, *107* (16), 3954–3962.

(50) Lu, J. R. Neutron reflection studies of interactions between surfactants and proteins at interfaces. *Annu. Rep. Prog. Chem., Sect. C: Phys. Chem.* **2002**, *98*, 3–32.

(51) Lu, J. R. Neutron reflection study of globular protein adsorption at planar interfaces. *Annu. Rep. Prog. Chem., Sect. C: Phys. Chem.* **1999**, *95*, 3–45.

(52) Lu, J. R.; Perumal, S.; Zhao, X.; Miano, F.; Enea, V.; Heenan, R. R.; Penfold, J. Surface-induced unfolding of human lactoferrin. *Langmuir* **2005**, *21*, 3354–3361.

(53) Lu, J. R.; Perumal, S.; Powers, E. T.; Kelly, J. W.; Webster, J. R. P.; Penfold, J. Adsorption of β-hairpin peptides on the surface of water: A neutron reflection study. *J. Am. Chem. Soc.* **2003**, *125*, 3751–3757.

(54) Lu, J. R.; Perumal, S.; Hopkinson, I.; Webster, J. R. P.; Penfold, J.; Hwang, W.; Zhang, S. Interfacial nano-structuring of designed peptides regulated by solution pH. *J. Am. Chem. Soc.* **2004**, *126*, 8940–8947.

(55) Fragneto, G.; Charitat, T.; Graner, F.; Mecke, K.; Perino-Gallice, L.; Bellet-Amalric, E. A fluid floating bilayer. *Europhys. Lett.* **2001**, *53* (1), 100–106.

(56) Fragneto, G.; Graner, F.; Charitat, T.; Dubos, P.; Bellet-Amalric, E. Interaction of the third helix of Antennapedia homeodomain with a deposited phospholipid bilayer: A neutron reflectivity structural study. *Langmuir* **2000**, *16*, 4581–4588.

(57) Lin, S.; Lee, C.-K.; Lin, Y.-H.; Lee, S.-Y.; Sheu, B.-C.; Tsai, J.-C.; Hsu, S.-M. Homopolyvalent antibody−antigen interaction kinetic studies with use of a dual-polarization interferometric biosensor. *Biosens. Bioelectron.* **2006**, *22*, 715–721.

(58) Wang, J.; Xu, X.; Zhang, Z.; Yang, F.; Yang, X. Real-time study of genomic DNA structural changes upon interaction with small molecules using dual-polarization interferometry. *Anal. Chem.* **2009**, *81*, 4914–4921.

(59) Moore, J. D.; Perez-Pardo, M. A.; Popplewell, J. F.; Spencera, S. J.; Raya, S.; Swann, M. J.; Shard, A. G.; Jones, W.; Hills, A.; Bracewell, D. G. Chemical and biological characterisation of a sensor surface for bioprocess monitoring. *Biosens. Bioelectron.* **2011**, *26*, 2940–2947.